Effect of Flap Sealing on Aerodynamic Characteristcs of the Wing Airfoil used at ITA's Unmanned Aerial Vehicle (UAV)

Tiago Barbosa de Araújo
Instituto Tecnológico de Aeronáutica (ITA). Praça Mal. Eduardo Gomes, 50, S J Campos – SP, Brasil
araujotb@ita.br

Roberto da Mota Girardi
Instituto Tecnológico de Aeronáutica (ITA). Praça Mal. Eduardo Gomes, 50, S J Campos – SP, Brasil
girardi@ita.br

André Valdetaro Gomes Cavalieri
Instituto Tecnológico de Aeronáutica (ITA). Praça Mal. Eduardo Gomes, 50, S J Campos – SP, Brasil
andre@ita.br

Abstract. *The unmanned aerial vehicle (UAV) considered in this work has the specific mission of examining elements of an electric energy transmission line (the tower, vegetation at the neighbor area and the electric cables). Such aircraft has some particular characteristics: (i) a relatively small velocity, that is, low Reynolds number, (ii) different material and manufacturing techniques are used and (iii) the weight is very low and, therefore, the aircraft will be very sensitive to atmospheric gusts. Such characteristic increases the difficulty to accomplish the mission, that is, performing a pre-defined path along a transmission line and its elements imaging. The present work objective is to obtain the aerodynamic characteristic curves (CL x α, CL x Cm e CL x CD) of the airfoil chosen to be used at the wing of the aircraft being developed. The experimental work will be performed at the ITA wind tunnel and the results will be corrected to consider the wind tunnel walls interference. Numerical results will be compared with experimental ones in order to perform a calibration of the numerical tool for the specific Reynolds number considered. Such calibration will be very useful because airfoil can be changed in more advanced design phases.*

Keywords*: Unmanned Aerial Vehicle, Airfoil, Experimental Method, Blockage effect, Numerical Solution*

1. INTRODUCTION

Unmanned aerial vehicles (UAV) can be used for several civil applications, such as: (i) Electrical lines and pipelines examination, (ii) harbors, forest reservations and less accessible frontiers vigilance, (iii) aircraft and disappeared people rescue, (iv) aerial picture generation and (v) others.

In 2004 Technological Institute of Aeronautics (ITA) was contacted to participate in a cooperation involving Advanced System Studies Center of Recife (CESAR) and São Francisco Electric Company (CHESF). The goal of such cooperation was an UAV development, for electrical line elements (towers, vegetation existing in the neighborhood of electrical lines, electrical connectors at the towers and etc) examination. In order to accomplish this task, a very low velocity (80 km/h) aircraft, flying at low altitude, is required, due to infrared camera limitations (required to observe hot spots, which indicate electric problems at some line elements). In such a velocity range the atmospheric gusts become very important owing to its effects on the flight security and because the electric line elements examination mission became very difficult, due to constant aircraft attitude changes.

The low aircraft velocity, required to accomplish the infrared camera examination mission, is in the inferior limit of an airplane flight envelope, because a high wing loading (W/S) is necessary to give the aircraft a low sensibility to atmospheric gusts, but, on the other hand, a low value of W/S is required to accomplish the low velocity flight requirement. All mission requirements could be fulfilled by using other kinds of aircrafts, like a helicopter, a dirigible or a hybrid vehicle, that is, a mixture between a dirigible and an airplane, for example. The most adapted kind of aircraft was analyzed by Girardi and Rizzi (2005a), where an airplane was chosen to be the kind of aircraft used in this project.

The second step in the conceptual phase of the airplane project was the definition of the more adapted configuration, considering all requirements fulfillment. Two basic airplane configurations were considered: (i) in the first one the engine is located at the airplane nose, a conventional tail was chosen to give stability and control to the aircraft and the camera was located at the fuselage low surface, near the aircraft gravity center (GC). (ii) In the second configuration, the engine was located at the fuselage tail, in the pusher configuration, and two booms were used to assembly the tail to the wing. In this configuration, the camera could be located at the fuselage nose or in the same place of the first configuration. Both configurations have high wing position (relative to the fuselage), a tricycle landing gear type and a rectangular wing. These configurations were analyzed by Girardi and Rizzi, (2005b) and the first one was chosen, considering the camera position near the aircraft GC (better to decrease effects on the camera due to the aircraft constant attitude changes, associated to the gusts effects) and the design team experience.

The aircraft conceptual design phase was executed by the Aeronautics Department of ITA and a special methodology was developed (Girardi e Rizzi, 2006) to face the problems associated to the airplane specific mission,

that is, image acquisition from an aircraft at low velocity, manufactured with non conventional material and subjected to atmospheric gusts, because of the low altitude required by the infrared imaging. In such methodology, the aircraft dimensions were determined considering the autopilot characteristics and this is an important aspect of the procedure adopted to this UAV design.

The work reported in this paper is inserted into the preliminary design phase, where more accurate information has to be used in order to improve the analysis methods used to determine the airplane dimensions, as well as, the relative positions of the different aircraft parts (wing, fuselage and tail). One of the problems verified during the conceptual design phase was the lack of information on low Reynolds number aerodynamic data, required to a small vehicle at low velocity. Such kind of information is very useful to generate the aircraft characteristic curves (CL x α, CL x Cm and the drag polar), which are used to performance, as well as, stability and control calculations.

In the present paper, aerodynamic data is presented to the airfoil chosen to the UAV wing, for low Reynolds number. A wind tunnel is used to determine the aerodynamic coefficients of a two element airfoil model, characterized with a 25% chord ratio flap. Initially, the flap deflection angle is kept at zero degrees and tests are performed to a set of angle of attacks to obtain the airfoil characteristic curves. The gap configuration, between the airfoil main element and its flap, can be changed in the following ways: (i) Sealed configuration, using a soft transition between the two elements, obtaining an external surface very similar to that one found in the airfoil without flap, (ii) a sealed configuration, performed by a continuous hinge axis along the model span. In this case, the shape variations at the gap region are exposed to the air flow. (iii) A non-sealed configuration. The three configurations were tested and their influences on the aerodynamic characteristic curves were obtained.

2 EXPERIMENTAL APPARATUS

The measurements were performed in a blower wind tunnel with square test section, characterized by a dimension of 460 mm. The flow velocity ranges from 4 to 30 m/s and the turbulence intensity is 0.5% at the maximum velocity. Along the test section length the cross section area is changed in order to compensate the boundary-layer growth and, as a consequence, to keep a constant static pressure. This area change is performed by filling the test section corners with triangular elements, whose dimension changes along test section length.

Lift, drag and pitch moment of a model are measured with a balance fixed at the test section lateral wall (outside the wind tunnel). Aerodynamic forces and moment on the model are transmitted to the balance through a metal axis. Such balance has a triangular plate used to fix the metal axis originated at the model. The triangular plate is connected to the wind tunnel structure by using three load cells (metal plates, instrumented with four strain gages each, in order to assembly a complete Wheatstone bridge). Two of these load cells are used to make measurement of lift and pitch moment (sensors A and F) and the third one is used to obtain drag force measurements (sensor D). Each load cell is connected to an independent signal conditioner module (amplifier and filter), which allows adjustment of the output voltage considering the data acquisition board characteristics. For the present experiment, the maximum output voltage of each sensor is chosen to be 10 volts, which maximize measurements resolution.

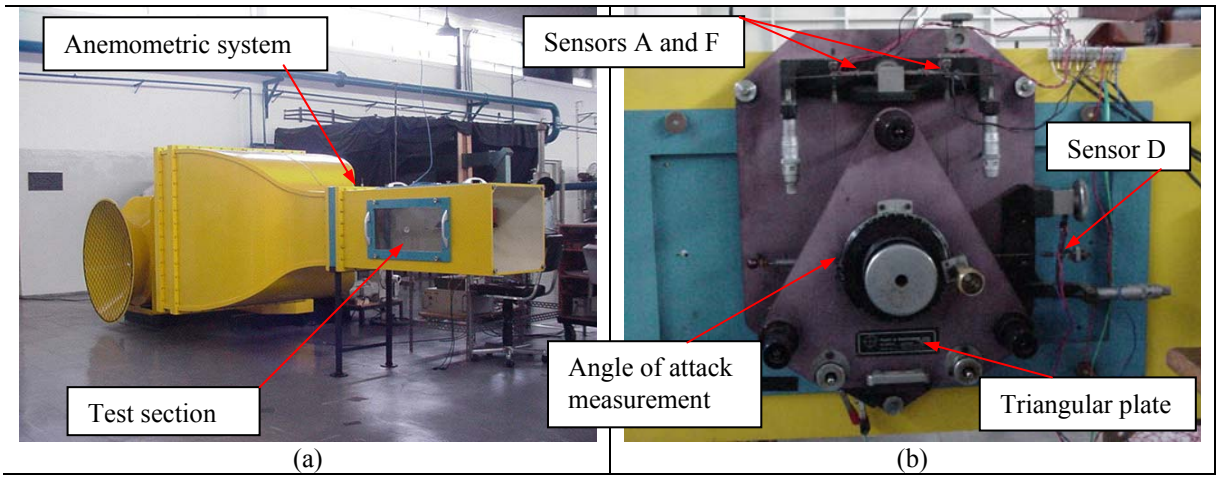

Figure 1: (a) Open circuit wind tunnel and (b) three components aerodynamic balance.

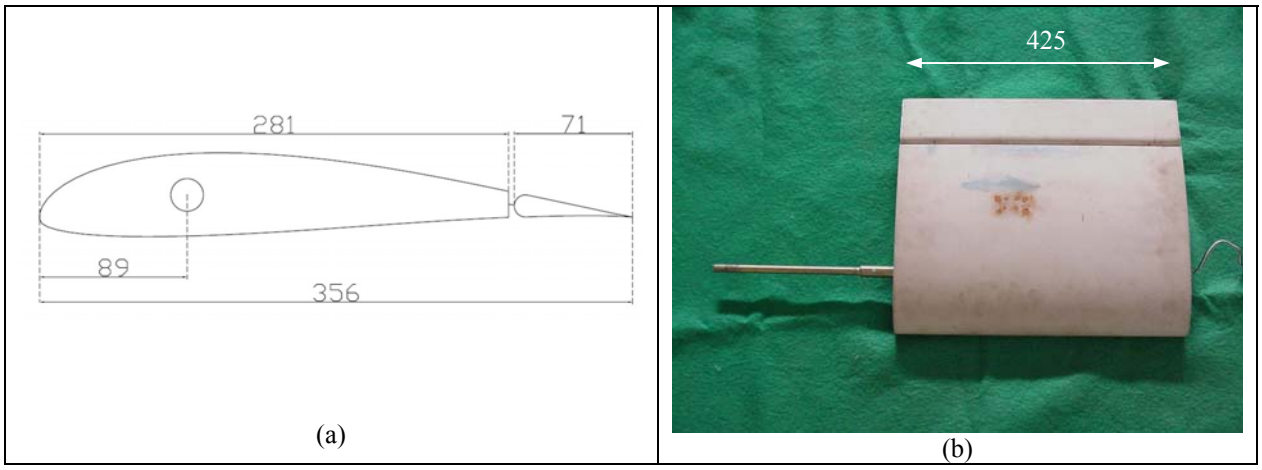

Figure 2: Airfoil and its flap: (a) lateral view and (b) plan view (from the top). Dimensions in mm.

The dynamic and static pressures are measured by using a Pitot tube located at the beginning of the test section (tunnel anemometric system), just after the end of the contraction section, as can be seen in the figure 1. Pressure transducers are connected to the Pitot tube and a signal conditioner is used to amplify the output voltages before the connection with the data acquisition board.

The model angle of attack is varied manually and its measurement is performed by a rotating device (where the model axis is fixed) divided in 360 equal parts. The uncertainty of ± 0.5 degrees can be considered to this measurement.

The Selig SD7062 airfoil with 20% chord ratio plain flap (see Fig. 2) was used as a model in the present work. It was manufactured with wood and its main dimensions are: 356 mm total chord, 425 mm spanwise dimension and 71 mm flap chord. The flap is connected to the main airfoil by using four plastic hinges, along the model span, and a gap of 3.5 mm was left between the airfoil two elements. A metal axis, used to connect the model to the balance, was fixed at 89 mm from the airfoil leading edge, as shown in the Fig. 3(a).

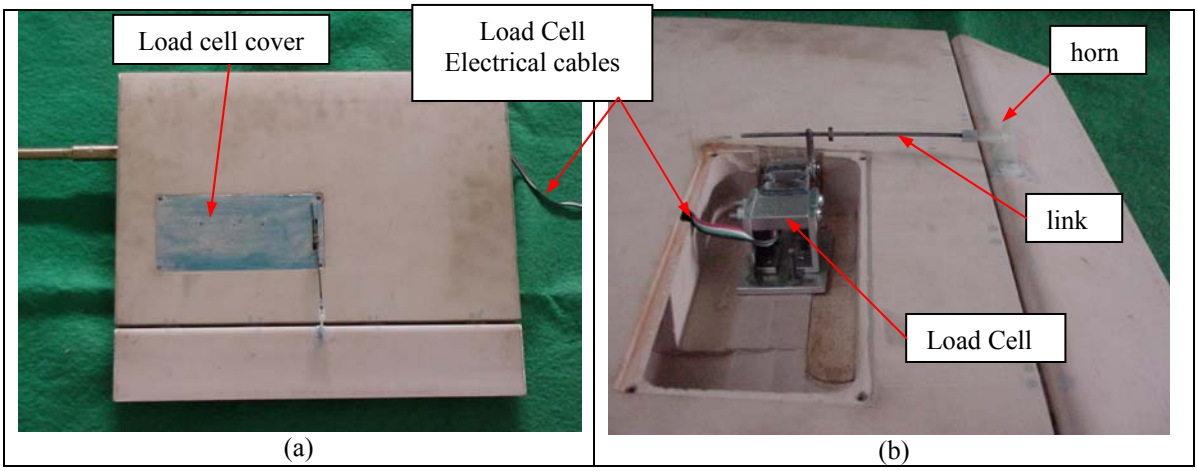

Figure 3: Hinge moment measurement apparatus: (a) lateral view and (b) plan view (from the bottom)

In order to make measurements of the flap hinge moment, a special apparatus was developed. A horn was fixed at the flap leading edge region (see Fig. 3a) and it was used to rotate the control surface around the hinges fixed to the main airfoil element. The main idea is to determine the force required to avoid the flap rotation and calculate hinge moment by using the distance from the hinge axis to the force application point. A small load cell, capable to make measurements of forces up to 5 kgf, was inserted inside the main element airfoil (see Fig. 3b) and a metal rod was used to link the load cell to the horn fixed at the airfoil flap, as shown in the Fig. 3b. This load cell is connected to a signal conditioner, through electric cables leaving the model by the extremity opposite to the metal axis used to fix the model to the aerodynamic balance. From the signal conditioner the signal is sent to the data acquisition board. Finally, a metal plate covers the force measurement apparatus in order to minimize the flow field disturbance, caused by the measurement device.

Once a cambered airfoil was chosen to be used at the UAV's wing, one important task to be performed in the aerodynamic tests is the initial alignment of the angle of attack. First of all, an axis is found parallel to the upper and lower test section walls and it is stamped on the end plates surfaces. Those axes are used to guide the fixation of model drawings, using chord line as a reference. When the airfoil is assembled inside the wind tunnel, the drawings fixed on

the two end plates surfaces are used to model alignment. The same drawings are used to establish the initial flap deflection, that is, deflection value when airfoil angle of attack and dynamic pressure are zero. Several lines, originated at the hinge axis and with different angles of flap deflection, are used to this initial deflection angle setup. The initial flap deflection angle is changed manually by using a system with two sows and a screw thread applied to the rod used as the link between the load cell and the horn fixed at the flap surface, as can be seen in the figure 3. Finally, it is important to note that the flap deflection is changed when wind tunnel is turned on and flap hinge moment cause small configuration distortion, due to the deformation on the load cell and on the rod. Such distortion has to be determined in order to correct the initial flap deflection. This task is performed during the load cell calibration procedure, as will be explained later in this paper.

End plates are used to isolate the wind tunnel boundary layer from the flow over the two dimensional model, in order to minimize three-dimensional flow, which is normally found at the model extremities (see Bearman, 1965). The experimental results reported by Kubo (1989), were used, initially, to define the end plates dimensions. The distance of the end plates are fixed from the wind tunnel lateral walls and it is defined as a function of the boundary layer thickness, determined in a previous work by using a hot wire anemometer.

After the first experiments with the model installed, a flow field between the two sides of the end plates was observed, generating a longitudinal vortex, whose intensity was increased with the airfoil angle of attack. The cause of such problem is the low pressure at the airfoil upper surface, associated to the flow established from the gap, between the test section wall and the end plate surface, and the region limited by the two end plates. Due to such flow a vortex is generated at the end plate upper edge. A similar vortex (with the same orientation) appears at the lower edge, caused by the high pressure at the airfoil inner surface. As the pressure difference increases with airfoil angle of attack, the longitudinal vortex intensities are incremented. The three-dimensional flow observed over the airfoil span (tufts visualization) is a consequence of the problem discussed above, which has to be minimized in order to determine reliable results for the two-dimensional model under study.

Considering the above paragraph analysis, the three-dimensional behavior along the model span could be minimized by using end plates spanning all the wind tunnel test section height (the airfoil is fixed at the horizontal position) in order to avoid the flow established along the upper and lower edges of the end plates. Due to the area variation along the wind tunnel test section (boundary layer compensation to keep static pressure constant along the test section length) the end plates have trapezoidal shape. Thin rubber strips are fixed along the upper and lower edges of the end plates and such edges are mounted flush to the test section corner surfaces, in order to guarantee a complete sealing between the regions mentioned above avoiding vortex formation.

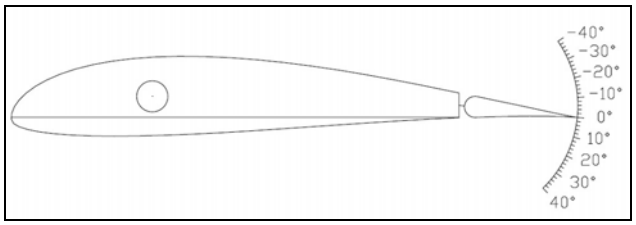

Figure 4: Airfoil main element and its flap drawing

3. EXPERIMENTAL PROCEDURE

In the present work, the following measurements have to be performed: (i) the forces and pitch moment of the complete model configuration, (ii) force required to determine the flap hinge moment and (iii) the dynamic pressure, necessary to obtain the non-dimensional coefficients for lift (Cl), drag (Cd), pitch moment (Cm). In this paper section, the experimental procedure established to determine each one of the above parameters is described, in order to show all care taken to guarantee reliable results.

As mentioned in the preceding section, lift, drag and pitch moment are measured by using an aerodynamic balance, with three load cells. The first task to be done is the load cells calibration, in order to obtain a correlation between the force acting on each load cell with the voltage read by the acquisition system. The calibration procedure is performed by incrementing loads from zero to the maximum value estimated for the specific sensor of the balance and, after that, a decrement is done up to zero again. At least 20 measures are used for the calibration process, in order to determine statistic parameters. During such procedure, a small amount of vibration is used to decrease the time required to the balance structural parts accommodation and it is worth to note that such vibration is kept during the sampling process, performed by the data acquisition system. In the calibration procedure, one thousand measures were performed during a sampling time of one second and just a value (average of 1000) of voltage is correlated to the force imposed on the load cell. Each balance sensor is loaded by using standard masses and a system constituted by cables and pulleys, responsible to apply the force to an axis connected to the balance, as can be seen in the figure 5. The three balance sensors are calibrated in two steps: (i) the load cell associated to the drag force is calibrated alone but (ii) for the other

two sensors, the vertical load applied to the axis connected to the balance is divided by two and the load cells associated to the lift and pitch moment are calibrated simultaneously.

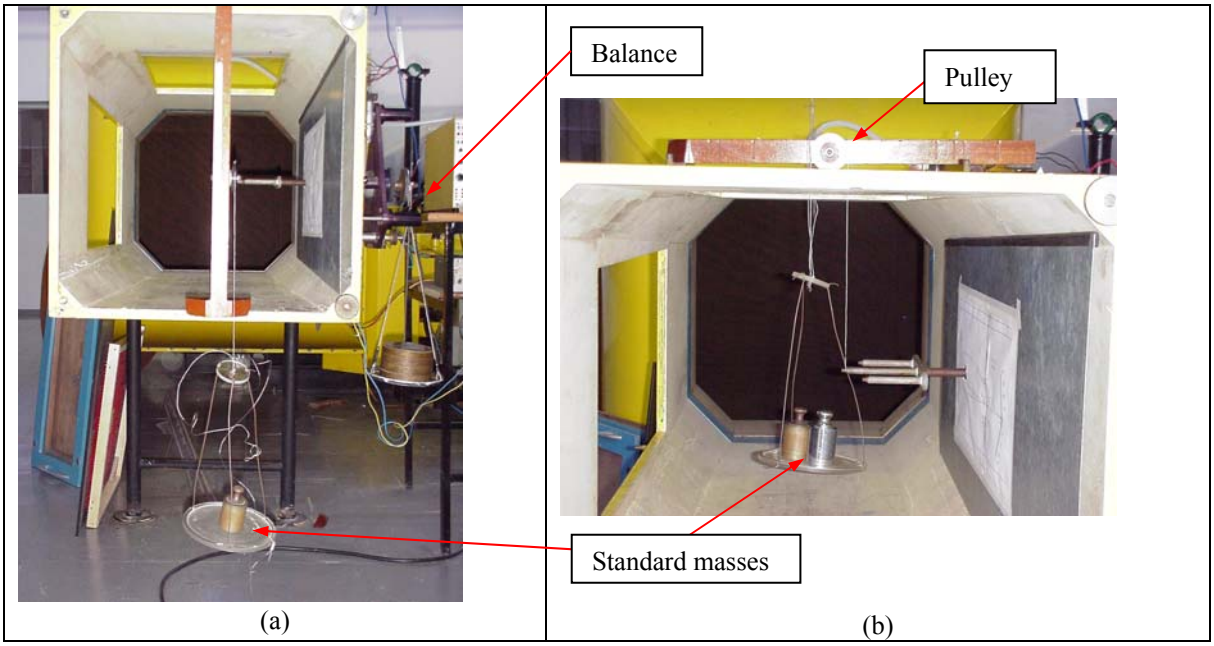

Figure 5: Aerodynamic balance calibration apparatus: (a) drag sensor and (b) Two other sensors used to obtain lift and pitch moment.

At the region where anemometric system is located (at the beginning of the test section) the flow field is distorted, due to the area variation along the contraction, causing errors in the values measured for the dynamic and static pressures. This problem can be corrected by performing a calibration procedure, where a Pitot tube, placed at the test section central region (location where models are tested) is compared with the anemometric system fixed at the wind tunnel. Calibration curves for the dynamic and static pressures are the results of the above procedure and they are used to correct the experimental results obtained with the wind tunnel anemometric system (The Pitot tube at the test section central region is withdrawn during the model experiments). The above calibration curves are incorporated in a computer code used to make calculations of the aerodynamic coefficients.

As mentioned in the previous section, the dynamic pressure is measured by using a pressure transducer, ranging from zero to 100 mm of water. A Betz manometer, with least count of 0,1 mm of water, is used as standard for the pressure transducer calibration, which is performed in the following way: (i) Initially, the pressure is increased and decreased several times (minimum of three) in order to get a repeatable measure of zero gage pressure at the Betz manometer. With such procedure, the internal walls of the Betz manometer are wetted. (ii) Starting from zero, the pressure is increased up to 50 mm of water, in steps of 5 mm and then (iii) pressure is decreased, using the same steps, up to zero again. For each point of the calibration curve, one thousand measures are collected during one second after the pressure stabilization (observed at the Betz manometer). The data acquisition code, written in LabView ambient, presents the linear fit of the experimental data and the standard deviations associated with the uncontrolled parameters of the experimental setup (random errors). These parameters are used to estimate the uncertainties associated to the aerodynamic coefficients.

After the calibration phase was finished, the experiment can be run in the following manner:

End plates are assembled inside the wind tunnel test section, the test section longitudinal axis are stamped on end plate surfaces and an airfoil (main and flap elements) drawings are fixed on the end plate surfaces, using the longitudinal axis and airfoil chord line to perform the airfoil drawing alignment.

Airfoil is fixed to the wind tunnel aerodynamic balance (through its metal axis) and initial alignment is performed, comparing the model with its drawing stamped on the end plate surfaces. The same comparison procedure is used to establish the initial flap deflection angle, which must be corrected as discussed before.

Before starting the wind tunnel, all sensor signals are read by the data acquisition system (initial voltages). This operation is performed after some vibration was introduced, in a similar manner used during the aerodynamic balance calibration (see preceding section), in order to guarantee all load cells are well accommodated to the loads associated the zero dynamic pressure. The initial voltage accuracies are very important because all force measurements accuracies depend on them. It is worth to note that the aerodynamic forces and moments are obtained through the difference between the sensor signals (voltage), measured with wind tunnel turned on, and the initial voltage (obtained with flow velocity equal to zero).

In the next step, wind tunnel is turned on and the dynamic pressure required to the specific test is established. The following results are typically obtained in an aerodynamic test program: The drag polar (Cd x CL), Cl x α and Cm x α, as well as, the hinge moment coefficient as a function of α, for a flap deflection angle. With the dynamic pressure fixed at a required value (associated to the Reynolds number) the angle of attack (α) is varied. In general, such variation starts at a negative angle of attack and increments of 2 degrees are used in the linear part of the lift curve. For greater values of α, increments of 1 degree are used for better description of the non linear flow behavior. Sometimes a decrement of α is performed to check hysteresis behavior.

During the experiments described at the two preceding topics, a data acquisition code, written in the LabView® ambient, is used to make the measurements of the aerodynamic balance sensors (three), the hinge moment sensor and the pressure transducer, used to register the wind tunnel dynamic pressure. For each angle of attack, whose value is inserted through the keyboard, the five sensor signals, mentioned above, are sampled 5000 times, using sampling rate of 1000 Hz. The resulting sample time of 5 seconds was chosen to account for the wind tunnel dynamic pressure variations and an average value is obtained for each parameter measured in this experiment.

Data reduction is performed with other code, also written in the LabView® ambient, where the data generated to each sensor (voltages) is combined with the calibration curves to determine forces and moments acting on the model. Ambient pressure and temperature are used to calculate air density and dynamic viscosity. These parameters are combined with the dynamic pressure to calculate the test Reynolds number. Finally, the model reference area (planform area) together with the forces and moments are used to determine the aerodynamic coefficients mentioned previously.

Data generated during calibration procedure, as well as during the experiment are used to determine the uncertainty associated to each aerodynamic coefficient. The uncertainty analysis was made by using the procedure described by Kline and McClintoch (1953).

4. ANALYSIS OF RESULTS

As we can see in fig. 2 the model utilized has a gap between the airfoil and its flap, and then to determine the influence of this gap on the aerodynamics coefficients we performed measurements, at the same Reynolds number, of the airfoil with three different configurations. These first setup consists on the airfoil shown in that figure with a plastic tape sealing the gap letting its surface continuous, like if the airfoil was without a flap. In the second configuration the tape is inserted in the gap simulating an infinite hinge that does not let the air flow pass through it. The last one is a configuration where we have two small plastic hinges linking the airfoil and the flap. In this configuration the air is let to pass throughout the gap, changing the flow backward the model, mainly with high angle of attack. To show the gap influence in the aerodynamics coefficients, figure 7 shows the graphic of the lift coefficient (CL) variation with the angle of the attack at the Reynolds number of $4{,}2\times10^{5}$.

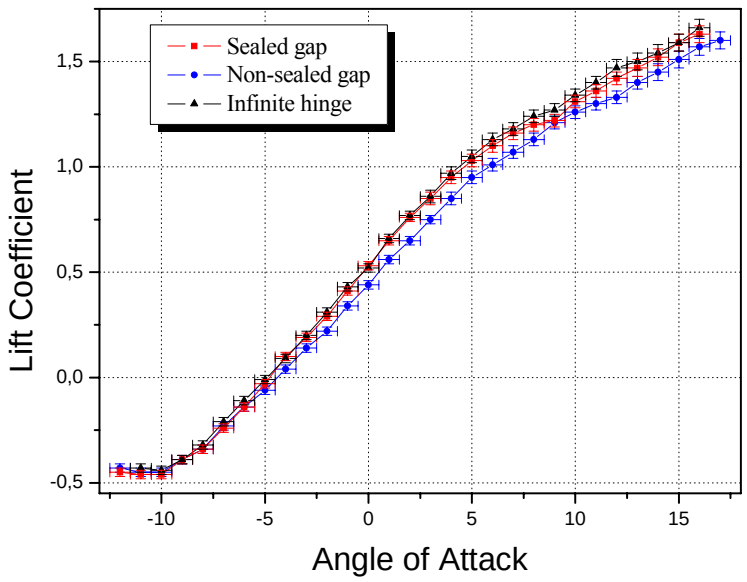

Figure 7: Variation of the Lift coefficient as a function of the angle of attack.

The results presented in this figures and in the others, in this work, as well as the tables results brings up with the probability of 95 % (2σ) and block rate corrected according to the procedure described by Gomes (2005), based on a panel method code. However, the correction method utilized here gives a correction for the range of linear C_L. Since all

values of the lift coefficient were corrected by the same method, the lift values of angles where boundary layer separation is present are not much reliable.

It was verified by visualizations with wool tufts that the boundary layer separation occurs only at the regions of the model closer to the side walls. These three-dimensional effects change greatly the stall characteristics of the airfoil. Future work will be developed in order to reduce the three-dimensional effects at the side walls, and to allow better experimental results for the non-linear range of lift coefficients.

In Figure 7 we can see that for this low Reynolds number the gap influence is small, but we can see an increase in the curve slope, in the linear part, of the $C_L(\alpha)$ for the two configuration where the air is not allowed to pass through the gap in relation of the non-sealed gap curve. In the gap, for the case of infinite hinge, we have recirculation regions which modify the flow and consecutively the aerodynamics coefficients; however it doesn't make so pronounced effects in the flow on the airfoil surface.

The difference among these two curves and the one with open gap can be explained by the fact that the gap region has a small pressure difference between the upper and the lower surfaces, since the pressure is continuous along the gap. As a consequence of this effect, there is no lift at the gap region. Both the sealed models do not allow flow through the model, and therefore have a greater lift at the sealed region. Then the fact of the non-sealed model presents the lowest slope is related to the flow through the gap that causes the boundary layer separation over some areas of the flap.

This result is of practical interest, since it shows the importance of sealing the gaps between the wing and the ailerons, between the horizontal tail and the elevator and the vertical tail and the rudder. If this procedure is not followed, a loss of almost 20% of the lift can occur for high angles of attack.

In the figure 8 a comparison is presented between the present experimental data, the experimental results of this airfoil by Selig et al (1995), and numerical results generated with XFOIL, a panel method code with boundary layer corrections developed by Drela (2007).

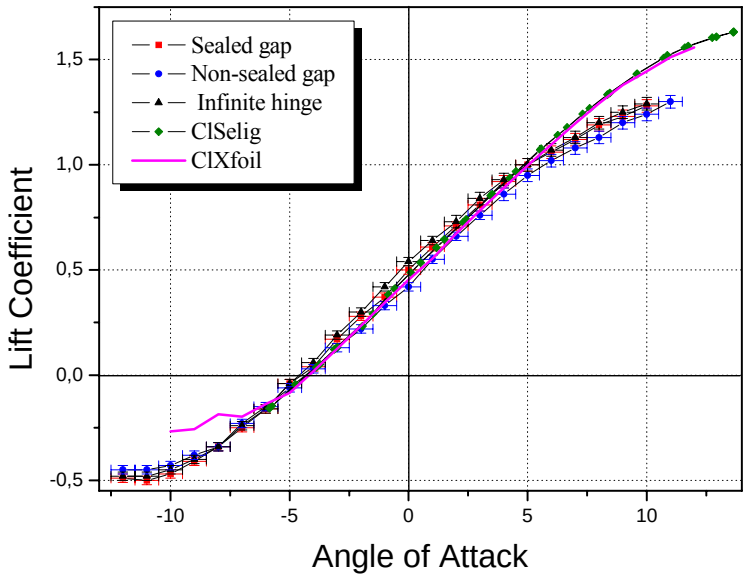

Figure 8: Comparison of the lift coefficient with XFOIL and other experimental results.

The observation of Figure 8 shows that the linear range of the present results are very close to the experimental values obtained by Selig et al (1995). Also, it can be noted that the numerical results are very accurate for this airfoil. This shows that XFOIL is a good tool for prediction of lift at this Reynolds number.

Figure 9 presents the drag coefficient variation with the angle of attack for the three configurations described before. As we have said to high angles of attack we get three-dimensional effects that change the flow over the airfoils and this makes our results for this range less reliable.

Also, the drag results were not corrected for blockage effects. However, since the three models have the same blockage, the comparison between the experimental values is valid.

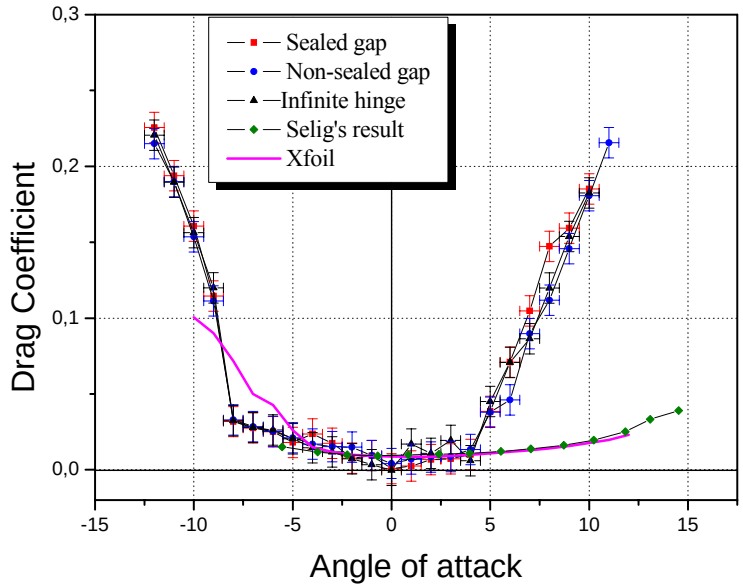

Figure 9: Drag coefficient versus angle of attack for the three configurations.

For low angles of attack we can see in this figure a small variation in the drag for the three configurations getting an overlap of the error bars. So we cannot make a better differentiation among the configurations drag for this range.

It is important to remark that the drag force was determined with a balance. This is not the best method for drag measurement, causing high uncertainties if the force is very small. This was the case here. Some error bars even cross the *x* axis, which does not have any physical meaning. Therefore, further experiments are required for an accurate determination of the drag coefficients. An experimental procedure that may be suitable for drag measurements is based on the integral equation for the momentum, with measurements across the wake of the airfoil in order to determine the aerodynamic forces.

The great differences between the present results for the drag and the experimental values of Selig et al (1995) are probably due to the formation of large separated zones at the side walls of the test section. The boundary layer separation increases largely the drag at this regions. Since the aerodynamic forces were measured with a balance, the determined drag coefficient rises significantly if there is separation at some sections.

Using the results presented in Figures 8 and 9, it is possible to obtain the experimental polar drag for the airfoil utilized at our UAV. This curve is shown in the figure 10.

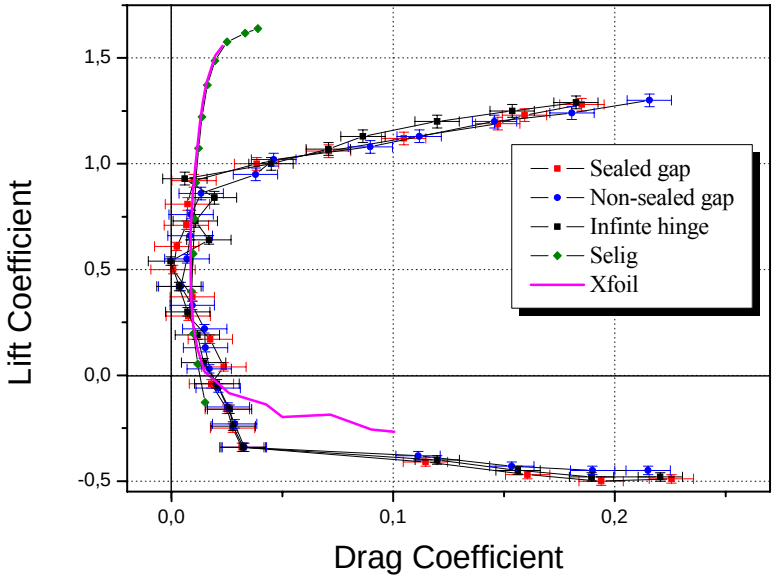

Figure 10: Experimental polar drag for the airfoil used at ITA's UAV.

As it was seen with the values of drag coefficient there is an overlapping of the curves for the region of lower values of drag. Again, the drag polar shows the necessity of using a different experimental procedure for measurements of drag.

The numerical results for the drag coefficient obtained with XFOIL showed a good agreement with the experimental values of Selig et al (1995), and with the present results for a range of small positive lift coefficients. Therefore this tool can also give good drag predictions for typical Reynolds numbers for UAVs.

Figure 11 shows the graphic of moment coefficient versus the lift coefficient which is used to determine the experimental aerodynamic center for the airfoil utilized at ITA's UAV wing.

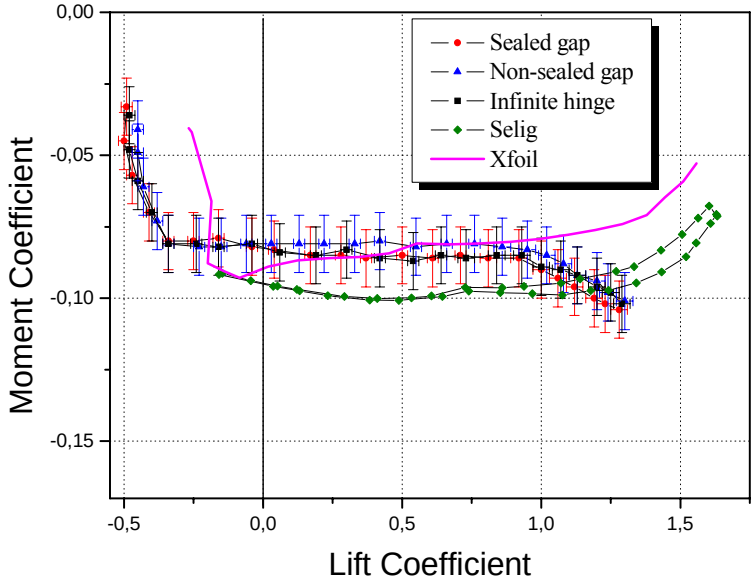

Figure 11: Graphic of C_M versus C_L.

The experimental results do not show significant differences among the C_M values of the three models. Thus, it is possible to conclude that the influence of the gap in the moment coefficient is small.

There are differences between the present results and the ones obtained by Selig et al (1995). The numerical results obtained with XFOIL better agreement with the present work. The results by Selig et al (1995) do not show an uncertainty analysis. It is possible that the combination of the present uncertainties with the ones that would be obtained for that work could explain the differences between the curves.

The behavior of the present results is different for high lift coefficients, since the obtained moment coefficient becomes more negative for high lift coefficients, and the opposite variation is perceived both in the results by Selig et al (1995) and the numerical values. This difference may also be caused by the three-dimensional effects at the tunnel side walls. However, further experiments, possibly with boundary layer blowing at the side walls, should be performed to investigate this effect.

From this curves we can calculate the aerodynamic center using the equation:

$$\frac{X_{AC}}{c} = -\frac{dC_M}{dC_L} + 0{,}25 \tag{1}$$

Where $\frac{dC_M}{dC_L}$ is obtained from a straight line adjustment on the middle region of the curves. In table 1 we have the results of the aerodynamic center position for the three configurations. To calculate it we have used the values comprehended between -1 and 7 degrees.

Table 1: Aerodynamic Center position for the each configuration described.

Configuration	Aerodynamic Center Position
Sealed	$0{,}25 \pm 0{,}03$
Non-sealed	$0{,}26 \pm 0{,}03$
Infinite hinge	$0{,}25 \pm 0{,}03$

From table 1 we can note that the aerodynamic center is in agreement with the position obtained by Selig et al (1995), which is of 24.6% of the chord.

5. FINAL REMARKS

The differences between the three tested models were perceived at the analysis of the lift coefficient. The loss of lift with an unsealed gap shows that the use of sealing is of great importance in aeronautics. The lift analysis also showed that a simple seal, following all the extension of the hinge, is able to maintain almost the same lift that would be generated by the airfoil without a control surface, which is represented by the sealed configuration. The present results for the drag coefficient are not conclusive, and further experiments are required, possibly with wake measurements. The moment coefficient did not show important differences between the models.

The lift and drag values obtained with XFOIL are accurate predictions, showing that this code is an efficient tool for the design of unmanned aerial vehicles.

6. ACKNOWLEDGEMENTS

To the Financiadora de Estudos e Projetos (FINEP), for supporting part of the resources used to the Unmanned Aerial Vehicle development (protocolo 243/2004) and to the Centro de Estudos de Sistemas Avançados do Recife (CESAR), to the partnership in this project. To the staff of the Prof. K.L. Feng Aeronautical Engineering Laboratory: Carlos Guedes Neto, Luis Zambrano Lara, Vitor Valentim Betti and Mario Correia.

7. REFERENCES

Bearman, P.W. (1965): Investigation of the flow behind a two-dimensional model with a blunt trailing edge and fitted with splitter plates. *J. Fluid Mech*., Vol. 28, pp. 241-255.

Drela, M., "XFOIL Subsonic Airfoil Development System". 28 Feb. 2007, <http://web.mit.edu/drela/Public/web/xfoil/>

Girardi, R.M. e Rizzi, P., (2005a), "Análise do tipo da aeronave mais adaptada para a inspeção de linhas de transmissão", Relatório de Trabalho, CESAR/ITA, 27 de junho.

Girardi, R.M. e Rizzi, P., (2005b), "Seleção da alternativa mais promissora para prova de conceito, através da construção e testes em vôo", Relatório de Trabalho, CESAR/ITA, 27 de junho.

Girardi, R.M. e Rizzi, P., (2006), "Desenvolvimento de Metodologia para Projeto Conceitual de um Veículo Aéreo Não Tripulado (VANT), Usado para Inspeção de Linhas de Transmissão de Energia Elétrica", Anais do Congresso Nacional de Engenharia Mecânica (CONEM), Recife, Pe.

Girardi, R.M. e Rizzi, P., (2006), "Projeto Conceitual de um Veículo Aéreo Não tripulado, Usado para Inspeção de Linhas de Transmissão de Energia Elétrica". Anais do 11º Encontro Nacional de Ciências e Engenharia Térmicas (ENCIT 2006), Curitiba, Dez. 5-8.

Gomes, C.D.A.N., (2005), "Avaliação da Razão de Bloqueio Bi-Dimensional Utilizando Método dos Painéis". Trabalho de Conclusão de Curso (Graduação) – Instituto Tecnológico de Aeronáutica, São José dos Campos.

Kline, S.J. and McClintock, F. A. (1953): Describing uncertainties in single-sample experiments. *Mechanical Eng*., pp. 3-8.

Kubo,Y. et all.(1989): Effects of end plates and blockage of structural members on drag forces. *J. Wind Eng. Ind. Aerodynamics*, vol.32, pp.329-342.

Rae, W.H. and Pope (1984), A *Low speed wind tunnel testing*. Second edition, John Wiley & Sons, USA.

Sousa, F.L. (1993): *Blockage ratio influence on the flow over two dimensional models*. Master Thesis, Instituto Tecnológico de Aeronáutica (ITA), S.J.Campos, SP, Brasil.

Raymer, D.P., (1999), "Aircraft design: a conceptual approach", AIAA Education Series, AIAA, Washington DC.

Roskam, J., (2000-2003), "Airplane design", parts I-VIII, Dar Corporation, Lawrence, Kansas, USA.

Selig S., Guglielmo, J. J., Broern, A. P., Giguerre, P, (1995), "Summary of Low-Speed Airfoil Data, vol. 1, 2 & 3". SoarTech Publications.

8. RESPONSIBILITY NOTICE

The authors are the only responsible for the printed material included in this paper.